Research Article Vol. 37, No. 6 / June 2020 / Journal of the Optical Society of America B 1911

Journal of the Optical Society of America B

OPTICAL PHYSICS

Klein tunneling of Dirac solitons in binary waveguide arrays

QUANG NGUYEN-THE[1] AND TRUONG X. TRAN[2,*]

[1]Department of Communications, Le Quy Don Technical University, 236 Hoang Quoc Viet str., 100000 Hanoi, Vietnam
[2]Department of Physics, Le Quy Don Technical University, 236 Hoang Quoc Viet str., 100000 Hanoi, Vietnam
*Corresponding author: tranxtr@gmail.com

Received 5 March 2020; revised 4 April 2020; accepted 1 May 2020; posted 4 May 2020 (Doc. ID 392263); published 1 June 2020

We systematically investigate the optical analog of the relativistic quantum Klein tunneling effect in binary waveguide arrays (BWAs) in the presence of Kerr nonlinearity where the Dirac solitons are used to construct the initial beams. The transmission coefficient of Dirac solitons obtained by direct beam propagation simulations in the low-power regime as a function of the potential step height and incidence angle is numerically shown for the first time, to the best of our knowledge, to be in excellent agreement with earlier predicted theoretical results in all ranges of parameters. The conditions for observing Klein tunneling are analytically derived and are also in excellent agreement with simulation-based results. We show that the nonlinearity in BWAs can severely influence the Klein tunneling effect. Our simulations show that initial beams based on Dirac solitons are much better candidates than Gaussian beams to quantitatively study the Klein tunneling effect in detail, especially in the regime where the incidence angle is very close to the Bragg angle.

https://doi.org/10.1364/JOSAB.392263

1. INTRODUCTION

The waveguide array (WA) is an excellent platform to study many peculiar and interesting discrete classic photonic phenomena, such as discrete diffraction [1,2], discrete solitons [1,3,4], the generation of so-called diffractive resonant radiation from discrete solitons [5], self-wavenumber shift of discrete solitons [6], and supercontinuum generation in both the frequency and wave number [7]. In applications, logic functions such as AND and NOT, and time gating function can be realized in waveguide arrays [8].

Moreover, some basic nonrelativistic quantum mechanics effects emerging from the Schrödinger equation, such as Zener tunneling [9] and Bloch oscillations [1,10,11], have been actively investigated through their photonic analogs in WAs. On the other hand, binary WAs (BWAs) are a wonderful system to simulate basic relativistic quantum mechanics effects originated from the Dirac equation, such as Zitterbewegung [12], Dirac solitons (DSs) in the nonlinear regime [13–18], and the topological Jackiw–Rebbi (JR) states [19,20]. The interaction between JR states and DSs in BWAs has been studied in Ref. [21]. The JR state [22] has paved the way for the prediction of the charge fractionalization effect, which is of primary importance in the fractional quantum Hall effect [23]. As expected, the topological JR states in BWAs are extremely robust under the influence of very strong disturbance [24]. Two JR states of different types in BWAs practically do not interact with each other at all, even though they are located quite close to each other [25]. This feature presents an efficient way to robustly guide optical signals in a network where various channels are tightly distributed. On the contrary, two JR states of the same type in BWAs can strongly couple to each other in the linear regime, and show the switching effect in the nonlinear regime as in fiber couplers [25].

Another extraordinary fundamental relativistic quantum mechanics effect called Klein tunneling (KT) has also been investigated in BWAs both theoretically [26] and experimentally [27]. KT refers to the prediction by Klein in 1929 [28] that relativistic fermions can tunnel through a repulsive potential step, whose height is greater than the particle energy, without the exponential damping governed by the Schrödinger equation. However, due to the extremely high field requirement, KT for relativistic electrons has not been observed experimentally yet. Moreover, to observe KT, the potential step must be very steep, i.e., the step must be realized at short distances comparable to the Compton wavelength [29].

Because KT is rooted in the Dirac equation, one can observe the analogs of KT in spinor-like systems possessing dispersion relations similar to those of relativistic electrons governed by a Dirac equation. For instance, in graphene the energy dispersion relation possesses a linear slope; as a result, charge carriers can undergo KT [30–33]. Due to that, demonstration of KT has been experimentally shown in graphene [34,35], in carbon nanotubes [36], and in optical traps for cold ions [37]. Remarkably, it has been shown in Ref. [37] that KT is

a wave effect, so it can be mimicked in a simple classical system. Therefore, several optical schemes have been proposed to directly observe KT by analyzing the light evolution in lattices of coupled waveguides, for instance, in 2D honeycomb photonic lattices [38], in planar BWAs [26,27], at the interface between positive-index and negative-index metamaterial media [39], and in an atomic ensemble with electromagnetically induced transparency [40]. It is interesting to note that KT in honeycomb lattices can be strongly suppressed by the electron–electron interaction [41], but only slightly by the nonlinearity [42]. These classical systems enable researchers to directly visualize KT.

In Refs. [26,27] KT has been investigated by launching a Gaussian beam into planar BWAs under incidence angles close to the so-called Bragg angles. However, it is well known that a Gaussian beam can propagate diffractionless, i.e., without distortion of its shape, only when it is launched into a uniform WA under the Bragg angle [43] in the linear regime. In other cases, the diffraction always happens to a Gaussian beam in the linear regime. Moreover, if a Gaussian beam is launched into planar BWAs under incidence angles quite close to the Bragg angles (which are necessary for converting the coupled-mode equations in BWAs into the Dirac equation), then the Zitterbewegung effect will immediately take place [12], and the Gaussian beam will be divided into two beams that both get broadened during propagation [see Fig. 5(e)]. The broadening of beams in this case can be suppressed by increasing the Gaussian beam incidence angle, as shown in Fig. 5(f). The broadening will be even more severe if the difference between the incidence angle and Bragg angle becomes smaller. In this case, in order to stop the broadening of the beam hitting the potential step, one needs to take an extremely large spatial width for the Gaussian beam at the input, which is not practical for experimental purposes. All this is not favorable for investigating KT. All these shortcomings of Gaussian beams can be overcome easily by using DSs at the input.

In this work, inspired by the earlier achievements in investigating KT in BWAs in Refs. [26,27] and also by the attractive properties of DSs in BWAs, we aim to study KT in BWAs in more detail with the use of DSs at the input. The paper is organized as follows. In Section 2, we summarize the theoretical results obtained earlier in Ref. [26], which will be verified for the first time, to the best of our knowledge, by direct simulation results later. In Section 3, we investigate thoroughly the influence of the potential step height on KT. In Section 4, we study the influence of the incidence wave number of DSs on KT. The influence of nonlinearity on KT is analyzed in more detail in Section 5. Finally, in Section 6, we summarize our results and finish with concluding remarks.

2. GOVERNING EQUATIONS AND TRANSMISSION OF LINEAR PLANE WAVES THROUGH A POTENTIAL STEP

Light evolution in a BWA with Kerr nonlinearity can be described in the continuous-wave regime by the following dimensionless coupled-mode equation (CME) [3,4,27,44]:

$$i\frac{da_n}{dz} = -\beta_n a_n - \kappa[a_{n+1} + a_{n-1}] + (-1)^n \sigma a_n - \gamma |a_n|^2 a_n, \tag{1}$$

where a_n represents the electric field amplitude in the waveguide with position n, z is the longitudinal spatial coordinate, κ and 2σ are the coupling coefficient and propagation mismatch between two adjacent waveguides in the BWA, respectively, and γ is the nonlinear coefficient of the waveguides. This model is reasonable when a wide beam in the continuous-wave regime is launched into the BWA where each waveguide supports a single mode. If pulses are used for excitation, one needs to take into account the waveguide dispersion as with the model in Ref. [17]. As in Ref. [27], the quantity β_n is introduced to represent an offset in propagation constants, which is necessary for including the potential step required for KT and is defined as $\beta_n = 0$ for all waveguides with $n < 0$ (region I) and $\beta_n = \beta_0$ for all waveguides with $n \geq 0$ (region II) [see Fig. 1(b)]. So, as seen from Eq. (1), the quantity $[\beta_n - (-1)^n \sigma]$ characterizes the propagation constant of the nth waveguide of the BWA whose transverse refractive index profile is schematically illustrated in Fig. 1(c). In the case of focusing nonlinearity, i.e., $\gamma > 0$, one can always normalize variables in the above dimensionless equation, such that both γ and κ are equal to unity. When a beam is launched into BWAs around the so-called Bragg angles, which correspond to the central spatial wave number of the beam $Q_B = \pm\pi/2$ [12], one can set $\Psi_1(n) = (-1)^n a_{2n}$ and $\Psi_2(n) = i(-1)^n a_{2n-1}$ [12,45], then introduce the continuous transverse coordinate $\xi \leftrightarrow n$ and the two-component spinor $\Psi(\xi, z) = (\Psi_1, \Psi_2)^T$, which satisfies the 1D nonlinear Dirac equation [13]

$$i\partial_z \Psi = V(\xi)\Psi - i\kappa\hat{\sigma}_x \partial_\xi \Psi + \sigma\hat{\sigma}_z \Psi - \gamma G, \tag{2}$$

where the nonlinear terms $G \equiv (|\Psi_1|^2\Psi_1, |\Psi_2|^2\Psi_2)^T$; $\hat{\sigma}_x$ and $\hat{\sigma}_z$ are the standard Pauli matrices. The potential step $V(\xi) = 0$ for $\xi < 0$ and $V(\xi) = \Phi_0 = -\beta_0 > 0$ for $\xi \geq 0$ [see Fig. 1(a)]. In quantum field theory, the parameter σ in the Dirac equation is often called the mass of the Dirac field (or Dirac mass). Without the nonlinear term, Eq. (2) is identical to Eq. (4) in Ref. [26], which is the well-known 1D Dirac equation for the

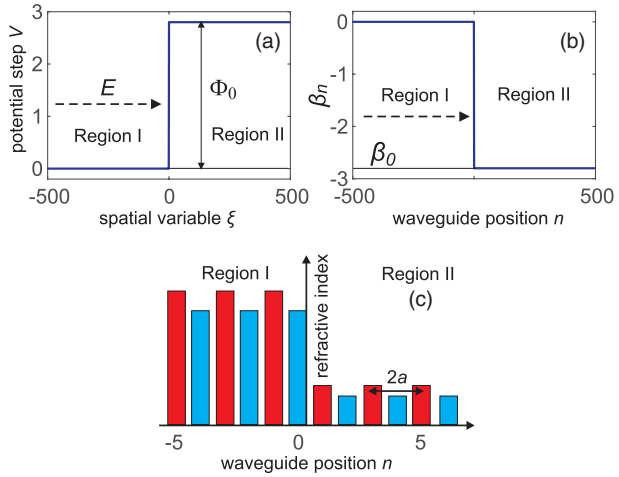

Fig. 1. (a) Scheme for investigating KT of a particle with energy E through a potential step $V(\xi)$ with potential step height $\Phi_0 > E$. (b) Propagation constant offset β_n introduced to a BWA to mimic the potential step $V(\xi)$. (c) Transverse refractive index profile of the BWA.

two-component spinor Ψ of a relativistic particle in the potential V, where z and ξ in Eq. (2) should be interpreted as the temporal t and spatial variables x, respectively {see Eq. (1) in Ref. [27]}. We also want to emphasize that in order to mimic the positive potential step $V(\xi)$ in the Dirac Eq. (2), the array β_n in Eq. (1) must have the profile as shown in Fig. 1(b), i.e., the parameter β_0 must be negative.

In Ref. [26], the transmission T of a plane wave through the potential step was derived based on Eq. (1) in the *linear* regime. In the rest of this section, we will re-introduce the main results regarding the transmission derivation in Ref. [26]. Suppose that the array β_n is independent of n and $\beta_n = \beta = -\Phi$; then, by making the Ansatz of a *plane wave* traveling in the plane (n, z) under some inclination,

$$a_n(Q) \sim \exp[i(Qn - \omega z)], \tag{3}$$

one can show that discrete coupled-mode Eq. (1) supports two minibands whose dispersion curves obey the following relations [44]:

$$\omega_{\pm}(Q, \Phi) = \Phi \pm \sqrt{\sigma^2 + 4\kappa^2 \cos^2 Q}, \tag{4}$$

where Q is the normalized wave number of the plane wave, which is equivalent to the quantity qa in Eq. (3) in Ref. [26] with a being the center-to-center distance between two adjacent waveguides in BWAs, and q is the wave number of the plane wave. For the sake of brevity, we will refer to Q just as wave number later. Obviously, the wave number Q is proportional to the angle of the beam propagation in BWAs, and represents the phase difference between two adjacent waveguides at a certain propagation distance z. Parameter ω can be interpreted as the energy (or frequency) of the plane wave if we recall the following transformations: $n \to \xi \to x, z \to t$.

Note that the dispersion relations in the form of Eq. (4) are obtained based on the discrete coupled-mode Eq. (1). Analogously, by making the Ansatz $\Psi \sim \exp[i(k\xi - \epsilon z)]$ for the continuous *linear* Eq. (2) (i.e., when $\gamma = 0$) with uniform potential Φ, one can obtain two branches for positive- and negative-energy states of the free relativistic electron {see Eq. (6) in Ref. [26]}:

$$\epsilon_{\pm}(k, \Phi) = \Phi \pm \sqrt{\sigma^2 + \kappa^2 k^2}. \tag{5}$$

Obviously, if the phase difference is written as $Q = \pm\pi/2 + k/2$ when k is small enough, then one can easily see that Eq. (4) can be approximately reduced to Eq. (5). So, now it is clearly seen that if the beam travels in the BWA around the Bragg angles of inclination, then Eq. (1) can be converted to the Dirac Eq. (2). Note again that the Bragg angle θ_B corresponds to the phase difference $Q_B = \pm\pi/2$ (see Ref. [12]).

Supposing that an incident plane wave belonging to the upper miniband ω_+ of the BWA travels in region I and has the incident wave number $Q_0 = \pi/2 + k_0/2$ with $0 < k_0 < \pi$, then this plane wave hits the potential step with the height $\Phi_0 = -\beta_0$. If this potential height is low enough, then we will observe the conventional damping of the transmitted wave as predicted by the nonrelativistic quantum Schrödinger equation. However, if the potential step is high enough, one can observe the optical analog of the relativistic quantum Klein tunneling based on Eq. (1). In this case, the transmitted wave will be another plane wave belonging to the lower miniband ω_- of the BWA traveling in region II [see also Figs. 4(a) and 4(c)] with a certain constant amplitude (instead of being damped), and with the transmitted wave number Q_1 obtained from the energy conservation condition

$$\omega_-(Q_1, \Phi_0) = \omega_+(Q_0, 0) \equiv \omega_0 \tag{6}$$

under condition $0 < Q_1 < \pi/2$, to make sure that the transmitted wave also has a positive group velocity. The power transmission coefficient T through the potential step is calculated as follows {see Eq. (7) in Ref. [26]}:

$$T = \frac{(\omega_0 - \sigma)(\omega_0 - \sigma - \Phi_0)\sin(2Q_0)\sin(2Q_1)}{[\Phi_0 \cos Q_0 \cos Q_1]^2 + [(\omega_0 - \sigma)\sin Q_0 \cos Q_1 + (\omega_0 - \sigma - \Phi_0)\sin Q_1 \cos Q_0]^2}. \tag{7}$$

The transmission coefficient T in the form of Eq. (7) is based on Eq. (1) for the discrete model in BWAs in the *linear* regime. The transmission coefficient T_D based on the Dirac Eq. (2) for the continuous model in the linear regime was calculated much earlier as follows (see, for instance, [46] and Eq. (A18) in Ref. [26]):

$$T_D = 1 - \left| \frac{-k_1(\epsilon_0 - \sigma) + k_0(\epsilon_0 - \sigma - \Phi_0)}{k_1(\epsilon_0 - \sigma) + k_0(\epsilon_0 - \sigma - \Phi_0)} \right|^2, \tag{8}$$

where k_0 and k_1 are the wave numbers of the incident and transmitted plane waves, respectively, which obey the following energy conservation relation:

$$\epsilon_0 \equiv \epsilon_+(k_0, 0) = \epsilon_-(k_1, \Phi_0), \tag{9}$$

with k_0 being positive and k_1 being negative to make sure that both incident and transmitted plane waves have positive group velocities.

3. RESULTS AND DISCUSSION

A. Klein Tunneling of Dirac Solitons through a Potential Step in BWAs: Influence of the Potential Step Height

In this section, we systematically investigate the influence of the potential step height Φ_0 on the transmission of an initial Dirac soliton under certain inclinations in BWAs. In a BWA made of materials with Kerr nonlinearity and without the potential step Φ_0, the analytical solution for DSs to the discrete coupled-mode Eq. (1) has been derived in Ref. [13] as follows:

$$\begin{bmatrix} a_{2n}(z) \\ a_{2n-1}(z) \end{bmatrix} = \begin{bmatrix} i^{2n} \frac{2\kappa}{w_0\sqrt{\sigma\gamma}} \operatorname{sech}\left(\frac{2n}{w_0}\right) e^{iz\left(\frac{2\kappa^2}{w_0^2\sigma} - \sigma\right)} \\ i^{2n} \frac{2\kappa^2}{w_0^2\sigma\sqrt{\sigma\gamma}} \operatorname{sech}\left(\frac{2n-1}{w_0}\right) \tanh\left(\frac{2n-1}{w_0}\right) e^{iz\left(\frac{2\kappa^2}{w_0^2\sigma} - \sigma\right)} \end{bmatrix}, \tag{10}$$

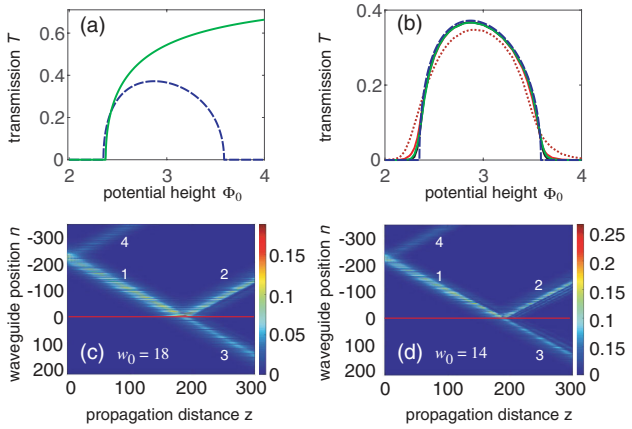

Fig. 2. (a) Theoretical transmission coefficients of a plane wave in the linear regime as a function of the potential step height Φ_0. The solid green curve in (a) is based on Eq. (8) for the continuous model, whereas the dashed blue curve in (a) is based on Eq. (7) for the discrete model. (b) Transmission coefficient of DSs in BWAs as a function of the potential step height: the solid red curve is obtained for an initial DS with $w_0 = 18$ and $\gamma = 1$; the solid black curve when $w_0 = 18$ and $\gamma = 0$; the solid green curve when $w_0 = 14$ and $\gamma = 0$; and the dotted brown curve when $w_0 = 14$ and $\gamma = 1$. The dashed blue curve in (b) is exactly the same theoretical curve as in (a). (c) Propagation of a DS in the nonlinear regime with $w_0 = 18$, $\gamma = 1$, and $\Phi_0 = 2.8$. (d) The same as (c), but now $w_0 = 14$. Other parameters: $k_0 = 0.3\pi$; $\sigma = 1$; $\kappa = 1$.

where w_0 characterizes the DS width. Note that the scheme for efficiently generating a DS in BWAs is proposed in Ref. [13]. The discrete gap solitons in BWAs have already been realized experimentally in Ref. [47]. Even though the DS in the form of Eq. (10) propagates along the longitudinal axis of the BWAs, it already has two central wave numbers $Q_B = \pm\pi/2$ [see Figs. 2(a) and 2(b) in Ref. [13]] corresponding to the Bragg angles $\pm\theta_B$ of the beam inclination. That is the reason that the DS in the form of Eq. (10) can help to convert the discrete coupled-mode Eq. (1) into the Dirac Eq. (2) even though this DS propagates *parallel* to the longitudinal axis. This is totally different from the conventional case where a plane wave in BWAs, or more practically a Gaussian beam, is used to mimic optical analogs of relativistic quantum effects emerging from the Dirac equation, for instance, the Zitterbewegung [12] and KT [26,27]. In the latter case, a Gaussian beam must be launched into the BWAs under angles close to the Bragg angle. This means that an initial Gaussian beam in the form

$$a_n \sim \exp\left(-\frac{n^2}{w_0^2}\right)\exp\left[i\left(\frac{\pi}{2}+\frac{k_0}{2}\right)n\right] \tag{11}$$

must be used to launch into the BWAs, where k_0 has a small positive value around zero, and w_0 also characterizes the Gaussian beam width.

On the contrary, in order to investigate the KT effect with the help of a DS at the input, one needs to use the following initial condition for the DS:

$$a_n^{\text{ini}} = a_n(0)\exp(ink_0/2), \tag{12}$$

where $a_n(0)$ in Eq. (12) is the DS solution taken at the distance $z = 0$ from Eq. (10), and k_0 also has a small positive value around zero. This initial condition in the form of Eq. (12) will be used in the rest of this work to investigate KT of DSs. Note also that the initial center of DSs in the form of Eq. (12) or Gaussian beams in the form of Eq. (11) is at the center of the array with $n = 0$, but it is quite easy to transversally shift this initial beam center.

In Fig. 2(a), we show the theoretical transmission coefficients T of a plane wave in the linear regime as a function of the potential step height Φ_0 when $k_0 = 0.3\pi$, and thus, the wave number $Q_0 = 1.3\pi/2$. The solid green curve in Fig. 2(a) is based on Eq. (8) for the continuous model, whereas the dashed blue curve in Fig. 2(a) is based on Eq. (7) for the discrete model. The other parameters used for obtaining the results shown in Fig. 2 are the following: the Dirac mass $\sigma = 1$, the coupling coefficient $\kappa = 1$, and the array consists of 1201 waveguides. As shown in Fig. 2(a), when the potential height $\Phi_0 < 2.35$, the transmission coefficient T obtained from both continuous and discrete models is equal to zero, which actually shows the damping regime of plane waves through potential steps that are not high enough, as predicted by the Schrödinger equation. However, if one slightly increases further the potential height Φ_0, then T sharply increases in both models due to KT. If Φ_0 is increased further, then one can observe the deviation between two curves shown in Fig. 2(a). Indeed, the dashed blue curve based on the discrete model of BWAs reaches the saturation for T, then decreases, and finally vanishes at the potential step height $\Phi_0 = 3.59$ and further. Meanwhile, the solid green curve based on the continuous model monotonically goes up (which, of course, cannot exceed unity if Φ_0 is increased further). The behavior of these two curves is explained in more detail in Fig. 4.

In Fig. 2(b), we plot the transmission coefficient T of DSs in BWAs as a function of the potential step height by using the direct beam propagation simulation as illustrated in Figs. 2(c) and 2(d). In Fig. 2(b), the solid red curve is obtained for an initial DS with the width parameter $w_0 = 18$ and the nonlinear coefficient $\gamma = 1$; the solid black curve is obtained for an initial DS with $w_0 = 18$ and $\gamma = 0$; the solid green curve is obtained for an initial DS with $w_0 = 14$ and $\gamma = 0$; and the dotted brown curve is obtained for an initial DS with $w_0 = 14$ and $\gamma = 1$. For comparison, we also add the theoretical dashed blue curve in Fig. 2(b), which is based on the discrete model in BWAs and is exactly the same as the curve of the same type in Fig. 2(a). We want to emphasize that this kind of comparison shown in Fig. 2(b) between the theoretical curve for T in BWAs and the numerical curves for T based on the beam simulation method is done for the first time. It is important to note that in order to obtain all numerical curves in Fig. 2(b), inclined DSs in the form of Eq. (12) with nonlinear coefficient $\gamma = 1$ are launched into BWAs, then this initial condition is used to integrate Eq. (1) to see the beam evolution where the nonlinear coefficient γ can be set equal to zero *only* during this integration process, as for the cases with the solid green curve and the solid black curve in Fig. 2(b). We have to mention this because we cannot use $\gamma = 0$ to calculate the initial DS in the form of Eq. (12), which is based on the *nonlinear* DS solution (10). As seen in Fig. 2(b), all numerical curves (except for the dotted brown curve) are in good agreement with the theoretical dashed blue curve with some

noticeable deviation only around the lower limit $\Phi_0 = 2.35$ and upper limit $\Phi_0 = 3.59$ for KT. Note that the theoretical result for T in Eq. (7) in BWAs is calculated for plane waves and in the linear regime, so in order to get closer to this theoretical curve, all numerical curves must be obtained in conditions similar to the two above-mentioned requirements. Thus, one needs to choose DSs with the beam width parameter w_0 being large to better satisfy the plane wave requirement, and set $\gamma = 0$ (i.e., in the linear regime) in integrating Eq. (1), as with the solid black curve and the solid green one in Fig. 2(b). Note also that although the solid red curve in Fig. 2(b) is obtained when $\gamma = 1$ in the integration process, but because this curve is obtained when an initial DS with a great beam width parameter $w_0 = 18$ is used, as shown in Eq. (10), the amplitudes of this DS are also small, and we operate in the quasi-linear regime. That is the reason that the solid red curve is also in good agreement with the theoretical dashed blue curve. On the contrary, although the dotted brown curve is also obtained with nonlinear coefficient $\gamma = 1$ being used for integrating Eq. (1), the beam width parameter $w_0 = 14$ of the DS is used in this case, which increases DS amplitudes, and thus enhances the nonlinear effect. That is the main reason that the deviation between this numerical curve and the theoretical one in Fig. 2(b) is the most significant. The influence of nonlinearity on KT will be investigated further in more detail in Section 5.

In Figs. 2(c) and 2(d), we show the evolution process when a DS in the form of Eq. (12) is launched into the BWAs in the nonlinear regime [i.e., $\gamma = 1$ for integrating Eq. (1)] with the incident wave number parameter $k_0 = 0.3\pi$, the potential step height $\Phi_0 = 2.8$, and the beam width parameters $w_0 = 18$ and 14, respectively. After launching the DS into BWAs, it is split into two beams labeled 1 and 4 in Figs. 2(c) and 2(d). Beam 1 later hits the potential step (whose position at the waveguide with $n = 0$ is illustrated by the red line) and is divided into the reflected beam with label 2 and the transmitted beam with label 3. The existence of beam 3 in Figs. 2(c) and 2(d) demonstrates KT. The ratio between the power of the transmitted beam 3 and the incident beam 1 is the transmission coefficient T, which is equal to 0.365 and 0.342 in Figs. 2(c) and 2(d), respectively. Note that the theoretical value for T in BWAs in the linear regime is $T = 0.37$.

In Figs. 3(a) and 3(b), we show the evolution process when a DS in the form of Eq. (12) is launched into the BWAs in the nonlinear regime with the incident wave number $k_0 = 0.3\pi$, beam width parameter $w_0 = 18$, and potential step heights $\Phi_0 = 2.0$ and 4.0, respectively. As shown in Fig. 2(b), the solid red curve representing these cases has $T = 0$. This is confirmed in Fig. 3, which shows that the incident beam 1 is completely reflected, and the transmitted beam through the potential step is not generated.

Now we want to answer one important question as to why there are both lower and upper limits of the potential step height Φ_0 for KT in BWAs, as shown by the dashed blue curve in Fig. 2(a). In Figs. 4(a) and 4(c), we plot the dispersion relation curves $\omega_\pm$ as functions of the wave number Q based on Eq. (4) in BWAs. The two solid curves in each of Figs. 4(a) and 4(c) show the two dispersion curves in region I when $\Phi_0 = 0$, whereas the two dashed curves show the two dispersion curves in region II when $\Phi_0 = 2.35$ [Fig. 4(a)] and $\Phi_0 = 3.59$ [Fig. 4(c)]. Note that all red curves in Figs. 4(a) and

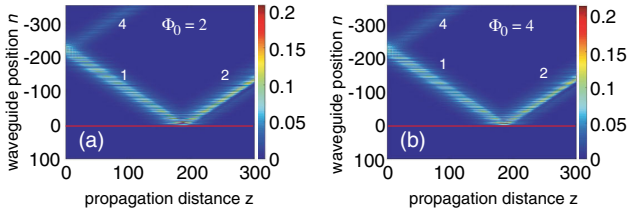

Fig. 3. (a), (b) Propagation of a DS in BWAs in the nonlinear regime with $w_0 = 18$, $k_0 = 0.3\pi$, and $\Phi_0 = 2$ and 4, respectively. Other parameters: $\sigma = 1; \kappa = 1$.

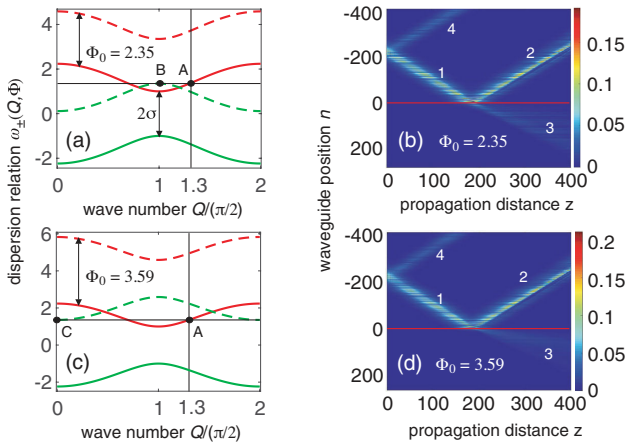

Fig. 4. (a) Band structure relation $\omega_\pm(Q, \Phi)$ when $\Phi = 0$ (solid curves) and $\Phi = \Phi_0 = 2.35$ (dashed curves) based on Eq. (4) for BWAs in the linear regime. (b) Propagation of a Dirac soliton in BWAs in the nonlinear regime ($\gamma = 1$) with $w_0 = 18$, $k_0 = 0.3\pi$, and $\Phi_0 = 2.35$. (c) The same as (a), but when $\Phi_0 = 3.59$. (d) The same as (b), but when $\Phi_0 = 3.59$. Other parameters: $\sigma = 1; \kappa = 1$.

4(c) represent the upper miniband ω_+, which is also called the positive-energy (or electron) branch, whereas all green curves therein represent the lower miniband ω_-, which is also called the negative-energy (or positron) branch [see Eq. (4)]. Let the incident plane wave hit the potential step with the incident wave number $Q_0 = 1.3\pi/2$ denoted by the vertical solid black line in Figs. 4(a) and 4(c), which crosses the upper miniband ω_+ at point A in region I with the potential $V = 0$. If region II has the potential $V = \Phi_0 = 2.35$, then point B on top of the lower miniband ω_- in region II now is on the same energetic level as point A; as a result, the energy conservation condition in the form of Eq. (6) is held true. In this case, the transmitted wave will have the wave number $Q_1 = \pi/2$ at point B, which obviously makes $T = 0$ as followed by Eq. (7) [because $\sin(2Q_1) = \sin(\pi) = 0$ now]. Thus, the potential step height $\Phi_0 \simeq 2.35$ is the lower limit of KT for this specific incident plane wave in the linear regime. As seen in Fig. 4(a), two points A and B must be on the same energetic level. From this condition, one can easily find the minimum analytical value of the potential step height for observing KT in BWAs in the linear regime $\Phi_0^{\min} = \sigma + \sqrt{\sigma^2 + 4\kappa^2 \cos^2 Q_0}$, which gives the value $\Phi_0^{\min} \simeq 2.35$ if $Q_0 = 1.3\pi/2$, as exactly depicted in Fig. 4(a).

If the potential step height $\Phi_0 < \Phi_0^{\min}$, then one cannot find any point belonging to the lower miniband ω_- in region II,

which is on the same energetic level as point A. Therefore, in this case, KT cannot occur, as predicted by the Schrödinger equation in nonrelativistic quantum mechanics.

Now we increase the potential step height further ($\Phi_0 > \Phi_0^{\min} \simeq 2.35$) while fixing the incident wave number $Q_0 = 1.3\pi/2$ and all other parameters. As shown in Fig. 4(a), one can easily find another point on the left of point B on the lower miniband ω_- in region II, such that this point is on the same energetic level as point A. This new point corresponds to the transmitted plane wave with $0 < Q_1 < \pi/2$, which must be satisfied to make sure that the transmitted wave has a positive group velocity. In this case, KT will take place with $T > 0$. If we increase further the potential step height to the value $\Phi_0 \simeq 3.59$ as shown in Fig. 4(c), then point C on the lower miniband ω_- in region II will be on the same energetic level as point A. In this case, the transmitted wave will have the wave number $Q_1 = 0$ at point C, which obviously makes $T = 0$ as followed by Eq. (7). This is the upper limit of Φ_0 for KT (with parameters used) because for higher values of Φ_0, obviously one again cannot find any point belonging to the lower miniband ω_- in region II, which is on the same energetic level as point A. As seen in Fig. 4(c), two points A and C must be on the same energetic level. From this condition, one can easily find the maximum analytical value of the potential step height for observing KT in BWAs in the linear regime $\Phi_0^{\max} = \sqrt{\sigma^2 + 4\kappa^2} + \sqrt{\sigma^2 + 4\kappa^2 \cos^2 Q_0}$, which gives the value $\Phi_0^{\max} \simeq 3.59$ if $Q_0 = 1.3\pi/2$, as exactly depicted in Fig. 4(c).

So, if an incident plane wave hits the potential step with the incident wave number $\pi/2 < Q_0 < \pi$, then the following condition for the potential step height Φ_0 must be held true if one wants to observe KT in BWAs in the linear regime:

$$\sigma + \sqrt{\sigma^2 + 4\kappa^2 \cos^2 Q_0} < \Phi_0 < \sqrt{\sigma^2 + 4\kappa^2} + \sqrt{\sigma^2 + 4\kappa^2 \cos^2 Q_0}. \tag{13}$$

Note that this condition for Φ_0 is explicitly provided here for the first time.

In Figs. 4(b) and 4(d), we show the propagation of beams when a DS is launched into BWAs in the nonlinear regime with the potential step heights $\Phi_0 = 2.35$ and 3.59, respectively. Other parameters for getting results in Figs. 4(b), 4(d) are as follows: $w_0 = 18$, $k_0 = 0.3\pi$ (thus $Q_0 = 1.3\pi/2$), and $\gamma = 1$. With DSs used at the input in Figs. 4(b) and 4(d) in the nonlinear regime, the transmission coefficients are calculated (based on the direct beam propagation simulation) to be $T = 0.0875$ and 0.0499, respectively, which correspond to some weak transmitted waves labeled 3 therein. These values of T are slightly different from zero (theoretical value) due to the fact that the plane wave and linear regime conditions are not held true. These conditions will be better satisfied if one uses DSs with a larger beam width parameter w_0, which will result in the decrease of T towards zero.

It is also easy to explain the behavior of the solid green curve in Fig. 2(a) governed by Eq. (8) for the continuous model. As mentioned above, when k is around zero, i.e., when the value of Q is around $\pi/2$, the dispersion curves governed by Eq. (4) are quite close to the two branches of the hyperbola governed by Eq. (5). With the incident wave number $Q_0 = 1.3\pi/2$, the potential step height $\Phi_0 \simeq 2.35$ is also the threshold for observing KT as shown for the case of the discrete model presented in Fig. 4(a). To be more accurate, by using Eq. (9), one can easily find the minimum analytical value of the potential step height for observing KT in the continuous model in the linear regime $\Phi_0^{\min} = \sigma + \sqrt{\sigma^2 + \kappa^2 k_0^2}$, which gives the value $\Phi_0^{\min} \simeq 2.37$ if $k_0 = 0.3\pi$ (or $Q_0 = 1.3\pi/2$, equivalently), as exactly depicted in Fig. 4(a). However, unlike the periodic curves with their finite maxima in the case of Eq. (4) where one period is shown in Fig. 4(a), two branches of the hyperbola governed by Eq. (5) go to $\pm\infty$ when the absolute value of k increases. That is the reason that, unlike the situation illustrated in Fig. 4(c) with the discrete model in BWAs, there is not an upper limit of Φ_0 for observing KT with the continuous model. In other words, for any arbitrary large value of Φ_0 that exceeds the threshold for observing KT, one can always find the transmitted wave number k_1 that satisfies the energy conservation condition in the form of Eq. (9); thus, there is just one threshold for the solid green curve in Fig. 4(a).

So, if an incident plane wave hits the potential step with the incident wave number parameter $0 < k_0 < \pi$, then the following condition for the potential step height Φ_0 must be held true if one wants to observe KT in the continuous model in the linear regime:

$$\Phi_0 > \sigma + \sqrt{\sigma^2 + \kappa^2 k_0^2}. \tag{14}$$

Note that for any value of Q_0 (and k_0), we must have $\Phi_0^{\min} > 2\sigma$ to observe KT both in the discrete and continuous models.

B. Klein Tunneling of Dirac Solitons through a Potential Step in BWAs: Influence of the Incident Wave Number

In this section, we analyze the influence of the incident wave number Q_0 on KT. In Fig. 5(a), we plot the transmission coefficient as a function of Q_0, where the dotted green and dashed blue curves represent the theoretical values of T in the linear case for the continuous and discrete models, respectively. These two theoretical curves as functions of the incidence angle (which is proportional to the incident wave number) are shown in Fig. 3 in Ref. [26]) for other sets of parameters. To check the accuracy of the dashed blue curve, we also plot the solid red curve in Fig. 5(a), which is obtained by the direct beam simulation method when a large DS is launched into BWAs in the nonlinear regime with $\gamma = 1$. As shown in Fig. 5(a), the numerical solid red curve is in good agreement with the theoretical dashed blue curve, the same as in Fig. 2(b), although the theoretical curve is obtained for plane waves in the linear regime in BWAs, whereas the numerical curve is based on a DS at the input in the nonlinear regime in BWAs. This is again possible because we use a large beam width parameter $w_0 = 18$ for the DS. Note that the comparison between the theoretical curve for T in BWAs as a function of the incident wave number and the simulations-based curve is also obtained for the first time in this work.

The limits of Q_0 for KT shown in Fig. 5(a) for two theoretical curves can be easily calculated. Let us first analyze the

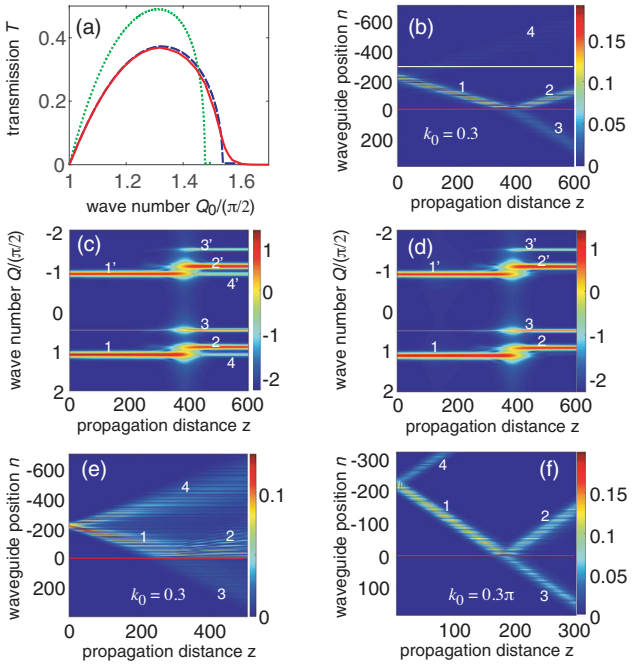

Fig. 5. (a) Transmission coefficient as a function of the incident wave number Q_0: the dotted green curve is based on Eq. (8) for the continuous model, the dashed blue curve is based on Eq. (7) for the discrete model, and the solid red curve is obtained by the direct beam simulation when a large DS is launched into BWAs with $\gamma = 1$. (b) Propagation of beams when a Dirac soliton is launched into BWAs in the nonlinear regime with $\gamma = 1$ and $k_0 = 0.3$. (c) Evolution of the spectrum in the (Q, z) plane. (d) The same as (c), but now the upper part of the beam above the white line in (b) is cut off. (e), (f) Propagation of a Gaussian beam in BWAs in the linear regime with $k_0 = 0.3$ and 0.3π, respectively. Other parameters: $\sigma = 1$; $\kappa = 1$; $w_0 = 18$; $\Phi_0 = 2.8$.

dashed blue curve in Fig. 5(a) representing KT in BWAs. As seen from Eq. (13), if the potential step height satisfies the condition $2\sigma < \Phi_0 < 2\sqrt{\sigma^2 + 4\kappa^2}$, then one can always observe KT with a certain value of Q_0 in the interval $(\pi/2, \pi)$, and Q_1 in the interval $(0, \pi/2)$, which satisfy Eq. (6). As clearly seen in Fig. 4(a), in this case, the lower limit of Q_0 for observing KT is $Q_0^{\min} = \pi/2$, because one always can find a corresponding value for the transmitted wave number Q_1. We need to find just the upper limit $Q_0^{\max}$, which is obviously the abscissa of point A in Fig. 4(a), because point A is on the same energetic level with the highest point of the green dashed curve therein [of course, in Fig. 4(a), if $\Phi_0 \neq 2.35$, then at point A, we have $Q_0 \neq 1.3\pi/2$]. As in Section 3, Eq. (6) will now have the following form for two points A and B: $\sqrt{\sigma^2 + 4\kappa^2}\cos^2 Q_0^{\max} = \Phi_0 - \sigma$. From this, one can easily get the upper limit $Q_0^{\max} = \text{acos}[-\sqrt{\Phi_0^2 - 2\Phi_0\sigma}/(2\kappa)]$, which gives the value $Q_0^{\max} \simeq 1.54\pi/2$ with parameters used for obtaining Fig. 5(a). This theoretical value of $Q_0^{\max}$ is in perfect agreement with the blue dashed curve in Fig. 5(a).

So, if the potential step height satisfies the condition $2\sigma < \Phi_0 < 2\sqrt{\sigma^2 + 4\kappa^2}$, then we will always observe KT in BWAs in the linear regime if the incident wave number satisfies the following condition:

$$\frac{\pi}{2} < Q_0 < \text{acos}\,\frac{-\sqrt{\Phi_0^2 - 2\Phi_0\sigma}}{2\kappa}. \tag{15}$$

Note that this condition for Q_0 is also explicitly provided here for the first time.

Analogously, by using Eq. (5) [or simply by using Eq. (14)], it is easy to show that if the potential step height satisfies the condition $\Phi_0 > 2\sigma$, then one will always observe KT in the continuous model in the linear regime if the incident wave number satisfies the following condition:

$$0 < k_0 < \frac{\sqrt{\Phi_0^2 - 2\Phi_0\sigma}}{\kappa}, \tag{16}$$

or, equivalently:

$$\frac{\pi}{2} < Q_0 < \frac{\pi}{2} + \frac{\sqrt{\Phi_0^2 - 2\Phi_0\sigma}}{2\kappa}. \tag{17}$$

If we take parameters used in Fig. 5(a), then we will find the condition $\pi/2 < Q_0 < 1.48\pi/2$, which is again in perfect agreement with the green dotted curve therein.

As an example, in Fig. 5(b), we show the evolution of $|a_n(z)|$ when a Dirac soliton is launched into BWAs in the nonlinear regime with $\gamma = 1$ and $k_0 = 0.3$, where the red line again indicates the position of the potential step at $n = 0$, and the white line indicates the waveguide with $n = -300$. The evolution of the Fourier transform of a_n along z is shown in Fig. 5(c). Each beam in Fig. 5(b) generates two spectrum bands with the distance between them equal to π. For instance, beam 1 in Fig. 5(b) generates two spectrum bands around $Q_0 = \pi/2 + 0.3 = 1.0955\pi/2$ with label 1, and $Q_0 = -0.9045\pi/2$ with label 1′ in Fig. 5(c) {see also Figs. 2(a) and 2(b) in Ref. [13] where a DS with $k_0 = 0$ is launched into BWAs}. The transmitted beam 3 in Fig. 5(b) generates two spectrum bands with labels 3 and 3' in Fig. 5(c), which are in perfect agreement with the theoretical value $Q_1 = \pi/2 + k_1/2 = 0.4884\pi/2$ as predicted by Eq. (6) and represented by the thin white line in Fig. 5(c). Analogously, beam 4 in Fig. 5(b) generates two spectrum bands with labels 4 and 4′ in Fig. 5(c). Note that the spectrum bands 1 and 4 are in the same position. This is also true for the spectrum bands 1′ and 4′. This can be easily checked as demonstrated in Fig. 5(d) where we show the evolution of the Fourier transform of a_n along z, but all the components a_n are now set to be zero above the white line at $n = -300$ in Fig. 5(b), i.e., the upper part of beam 4 is cut off. As clearly seen in Fig. 5(d), now we do not observe two spectrum bands with labels 4 and 4′ anymore.

We want to emphasize that with a DS at the input, one can easily investigate KT for all ranges of the incident wave number Q_0, including the values Q_0 around $\pi/2$ where it is quite problematic with a Gaussian beam at the input. Indeed, as illustrated in Fig. 5(e), a Gaussian beam with $k_0 = 0.3$ (so $Q_0 = 1.0955\pi/2$) and beam width parameter $w_0 = 18$ is launched into BWAs in the linear regime. Four beams with labels 1–4 are generated in Fig. 5(e), but all of them quickly spread out, which makes it impossible to verify Eq. (7) obtained for plane waves. In this case, one needs to take a very large value for the beam width parameter w_0 to obtain collimated beams during propagation. However, the same Gaussian beam, but

with $k_0 = 0.3\pi$ (or $Q_0 = 1.3\pi/2$), can help to verify Eq. (7) quite easily, as shown in Fig. 5(f). Note that because the peak amplitudes for the Gaussian beams in Figs. 5(e) and 5(f) are quite small, if we use $\gamma = 0$ (linear regime) or $\gamma = 1$ (nonlinear regime), the beams' evolution therein will only slightly change.

C. Klein Tunneling of Dirac Solitons through a Potential Step in BWAs: Influence of Nonlinearity

In the rest of this work, we investigate the influence of nonlinearity on KT. So far, this problem has been touched on in just a few works. Unlike the situation with KT in honeycomb lattices, which is only slightly affected by nonlinearity [42], we show that the nonlinearity can have a significant impact on KT in BWAs.

First, we want to note that if we replace the nonlinear coefficient $\gamma \to m\gamma$ for any value of the *non-zero* factor $m > 0$ while fixing all other parameters in Eq. (1), then as easily seen from Eq. (1), the field components will be simply scaled as follows: $a_n(z) \to a_n(z)/\sqrt{m}$. That is why the DS solution in the form of Eq. (10) must be inversely proportional to $\sqrt{\gamma}$. In other words, the beam dynamics must be the same if we multiply γ in Eq. (1) by a positive factor m, and at the same time take the initial conditions in the form of Eq. (10) with the new value of γ. This is confirmed by comparing Fig. 2(c) with Fig. 6(a) where all parameters are the same except that the nonlinearity coefficient $\gamma = 1$ in Fig. 2(c), but $\gamma = 100$ in Fig. 6(a) is used for integrating Eq. (1) with the initial conditions taken in the form of Eq. (10), which are now also scaled down with the corresponding value of $\gamma = 100$ at the same time. As expected, all details in Figs. 2(c) and 6(a) are exactly the same, with the only difference in scales for color bars [the scale of the color bar in Fig. 6(a) is 10 times smaller than the one in Fig. 2(c), as predicted]. As a result, the transmission coefficient T in Fig. 6(a) must be equal to 0.365, i.e., the same as in Fig. 2(c).

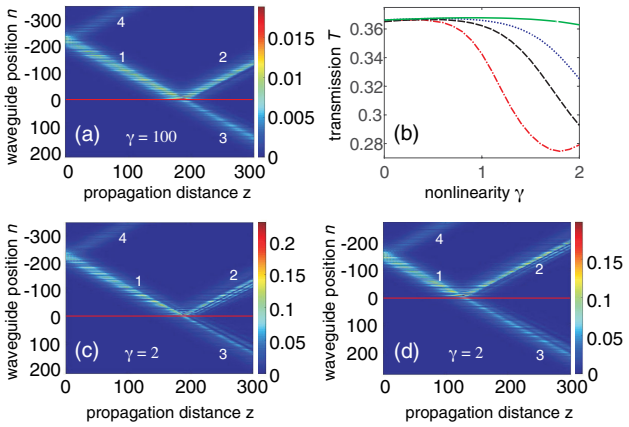

Fig. 6. (a) Propagation of a DS with $w_0 = 18$ when $\gamma = 100$. (b) Transmission coefficient T as a function of the nonlinearity coefficient γ: the solid green curve and dotted blue curve are obtained with $w_0 = 18$, and the initial DS center at $n = -150$ and -220, respectively; the dashed black curve and dashed-dotted red curve are obtained with $w_0 = 14$, and the initial DS center at $n = -150$ and -220, respectively. (c), (d) Propagation of a Dirac soliton with the initial center at $n = -220$ and -150, respectively, in the case where $w_0 = 18$ and $\gamma = 2$. Other parameters: $k_0 = 0.3\pi$; $\Phi_0 = 2.8$;$\sigma = 1$; $\kappa = 1$.

Now we want to analyze a different situation where the nonlinear coefficient $\gamma = 1$ is *fixed* for getting the initial conditions in the form of Eq. (10), but the value of γ can be changed while integrating Eq. (1). This situation can be interpreted as the case where the same input signal is used for different BWAs with various γ. In Fig. 6(b), we plot the transmission coefficient T as a function of γ, where the solid green curve and dotted blue curve are obtained with the beam width parameter $w_0 = 18$, and the initial DS centers at $n = -150$ and -220, respectively; the dashed black curve and dashed-dotted red curve are obtained with $w_0 = 14$, and the initial DS centers at $n = -150$ and -220, respectively. All curves in Fig. 6(b) have some common features:

(i) they first slightly increase as γ increases, then they begin to decrease if γ increases further;
(ii) the influence of γ will be less pronounced if the beam width parameter w_0 is large (this is also expected because when w_0 is large, the DS peak amplitude is low, which makes the nonlinearity less important);
(iii) the transmission T in the nonlinear regime also depends on the distance traveled by a DS before it hits the potential step, especially when γ is larger than unity.

To illustrate the influence of the distance traveled by a DS before it hits the potential step, we show the beam dynamics in Figs. 6(c) and 6(d) where two DSs are launched into BWAs under exactly the same conditions except for the fact that the initial DS center is located at $n = -220$ and -150, respectively. The value of T is calculated to be 0.3252 and 0.3629 through direct simulation data in Figs. 6(c) and 6(d), respectively. Note that the theoretical value $T = 0.3699$ is obtained for the discrete model based on Eq. (7) in the linear regime for parameters used in Figs. 6(c) and 6(d). The influence of the initial DS center on KT is understandable, even for DSs with a large value of $w_0 = 18$, as in Figs. 6(c) and 6(d). Indeed, as the initial condition for the input DS is taken with fixed $\gamma = 1$, as long as we increase from unity for the value of γ in Eq. (1) for beam evolution simulation, the fixed input condition will be more and more different from the ideal condition to get collimated beams during propagation. At the first stage, beam 1 in Fig. 6(d) can still be considered as a parallel beam. However, at the later stage before hitting the potential step, beam 1 in Fig. 6(c) is not parallel anymore, but propagates in an unpredictable manner when the central part of the beam undergoes the self-focusing effect due to nonlinearity. On the contrary, when γ is close to zero, as clearly seen in Fig. 6(b), the influence of γ on the transmission T is less noticeable, because in this quasi-linear case, the beams undergo just a slight broadening if the initial DS beam width is large enough.

4. CONCLUSION

We have systematically investigated the optical analog of the relativistic quantum KT effect of DSs through a potential step in BWAs with Kerr nonlinearity. The transmission coefficient of DSs through the potential step is calculated via the beam propagation simulation and is demonstrated for the first time to be in excellent agreement with the theoretical results in the linear regime for the same model if the beam width of DSs is

large enough. The influence of the potential step height and the incident wave number of DSs on KT has been investigated systematically, which helps to confirm the validity of the theoretical results of the transmission coefficient in BWAs. The limits of the potential step height and the incident wave number for observing KT in the linear regime for both discrete and continuous models have been exactly derived in the analytical forms for the first time. The nonlinearity of the system can have significant impact on the KT effect and can dramatically decrease the transmission coefficient as compared to its theoretical values in the linear regime. Our results show that DSs are a great candidate for studying the optical analog of the KT effect and other relativistic quantum effects in BWAs in wide ranges of parameters.

Funding. National Foundation for Science and Technology Development (102.04-2015.22).

Disclosures. The authors declare no conflicts of interest.

REFERENCES

1. D. N. Christodoulides, F. Lederer, and Y. Silberberg, "Discretizing light behaviour in linear and nonlinear waveguide lattices," Nature **424**, 817–823 (2003).
2. A. L. Jones, "Coupling of optical fibers and scattering in fibers," J. Opt. Soc. Am. **55**, 261–271 (1965).
3. D. N. Christodoulides and R. I. Joseph, "Discrete self-focusing in nonlinear arrays of coupled waveguides," Opt. Lett. **13**, 794–796 (1988).
4. Y. S. Kivshar and G. P. Agrawal, *Optical Solitons: from Fiber to Photonic Crystals*, 5th ed. (Academic, 2003).
5. Tr. X. Tran and F. Biancalana, "Diffractive resonant radiation emitted by spatial solitons in waveguide arrays," Phys. Rev. Lett. **110**, 113903 (2013).
6. Tr. X. Tran and F. Biancalana, "Mimicking the nonlinear dynamics of optical fibers with waveguide arrays: towards a spatiotemporal supercontinuum generation," Opt. Express **21**, 17539–17546 (2013).
7. Tr. X. Tran, D. C. Duong, and F. Biancalana, "Supercontinuum generation in both frequency and wave number domains in nonlinear waveguide arrays," Phys. Rev. A **89**, 013826 (2014).
8. D. N. Christodoulides and E. D. Eugenieva, "Blocking and routing discrete solitons in two-dimensional networks of nonlinear waveguide arrays," Phys. Rev. Lett. **87**, 233901 (2001).
9. M. Ghulinyan, C. J. Oton, Z. Gaburro, L. Pavesi, C. Toninelli, and D. S. Wiersma, "Zener tunneling of light waves in an optical superlattice," Phys. Rev. Lett. **94**, 127401 (2005).
10. T. Pertsch, P. Dannberg, W. Elflein, A. Bräuer, and F. Lederer, "Optical Bloch oscillations in temperature tuned waveguide arrays," Phys. Rev. Lett. **83**, 4752–4755 (1999).
11. G. Lenz, I. Talanina, and C. M. de Sterke, "Bloch oscillations in an array of curved optical waveguides," Phys. Rev. Lett. **83**, 963–966 (1999).
12. F. Dreisow, M. Heinrich, R. Keil, A. Tünnermann, S. Nolte, S. Longhi, and A. Szameit, "Classical simulation of relativistic Zitterbewegung in photonic lattices," Phys. Rev. Lett. **105**, 143902 (2010).
13. Tr. X. Tran, S. Longhi, and F. Biancalana, "Optical analogue of relativistic Dirac solitons in binary waveguide arrays," Ann. Phys. **340**, 179–187 (2014).
14. Tr. X. Tran, X. N. Nguyen, and D. C. Duong, "Dirac soliton stability and interaction in binary waveguide arrays," J. Opt. Soc. Am. B **31**, 1132–1136 (2014).
15. Tr. X. Tran and D. C. Duong, "Higher-order Dirac solitons in binary waveguide arrays," Ann. Phys. **361**, 501–508 (2015).
16. Tr. X. Tran, X. N. Nguyen, and F. Biancalana, "Dirac solitons in square binary waveguide lattices," Phys. Rev. A **91**, 023814 (2015).
17. Tr. X. Tran and D. C. Duong, "Dirac light bullets in nonlinear binary waveguide arrays," Chaos **28**, 013112 (2018).
18. Tr. X. Tran, "Switching a Dirac soliton by a weak signal in binary waveguide arrays with varying propagation mismatch," J. Opt. Soc. Am. B **36**, 2001–2006 (2019).
19. Tr. X. Tran and F. Biancalana, "Linear and nonlinear photonic Jackiw-Rebbi states in interfaced binary waveguide arrays," Phys. Rev. A **96**, 013831 (2017).
20. Tr. X. Tran, H. M. Nguyen, and D. C. Duong, "Jackiw-Rebbi states in interfaced binary waveguide arrays with Kerr nonlinearity," Phys. Rev. A **100**, 053849 (2019).
21. Tr. X. Tran, D. C. Duong, and F. Biancalana, "Interaction between Dirac solitons and Jackiw-Rebbi states in binary waveguide arrays," J. Lightwave Technol. **35**, 5092–5097 (2017).
22. R. Jackiw and C. Rebbi, "Solitons with fermion number 1/2," Phys. Rev. D **13**, 3398–3409 (1976).
23. R. B. Laughlin, "Nobel lecture: fractional quantization," Rev. Mod. Phys. **71**, 863–874 (1999).
24. Tr. X. Tran, "Extreme robustness of Jackiw-Rebbi states in binary waveguide arrays under strong disturbance," J. Opt. Soc. Am. B **36**, 2559–2563 (2019).
25. Tr. X. Tran, "Coupling and protection effects of Jackiw-Rebbi states and trivial states in interfaced binary waveguide arrays" (to be published).
26. S. Longhi, "Klein tunneling in binary photonic superlattices," Phys. Rev. B **81**, 075102 (2010).
27. F. Dreisow, R. Keil, A. Tünnermann, S. Nolte, S. Longhi, and A. Szameit, "Klein tunneling of light in waveguide superlattices," Europhys. Lett. **97**, 10008 (2012).
28. O. Klein, "Die Reflexion von Elektronen an einem Potentialsprung nach der relativistischen Dynamik von Dirac," Z. Phys. **53**, 157–165 (1929).
29. F. Sauter, "Über das Verhalten eines Elektrons im homogenen elektrischen Feld nach der relativistischen Theorie Diracs," Z. Phys. **69**, 742–764 (1931).
30. K. S. Novoselov, A. K. Geim, S. V. Morozov, D. Jiang, M. I. Katsnelson, I. V. Grigorieva, S. V. Dubonos, and A. A. Firsov, "Two-dimensional gas of massless Dirac fermions in graphene," Nature **438**, 197–200 (2005).
31. M. I. Katsnelson, K. S. Novoselov, and A. K. Geim, "Chiral tunnelling and the Klein paradox in graphene," Nat. Phys. **2**, 620–625 (2006).
32. S. Y. Zhou, G.-H. Gweon, J. Graf, A. V. Fedorov, C. D. Spataru, R. D. Diehl, Y. Kopelevich, D.-H. Lee, S. G. Louie, and A. Lanzara, "First direct observation of Dirac fermions in graphite," Nat. Phys. **2**, 595–599 (2006).
33. C. W. J. Beenakker, "Colloquium: Andreev reflection and Klein tunneling in graphene," Rev. Mod. Phys. **80**, 1337–1354 (2008).
34. A. F. Young and P. Kim, "Quantum interference and Klein tunnelling in graphene heterojunctions," Nat. Phys. **5**, 222–226 (2009).
35. N. Stander, B. Huard, and D. Goldhaber-Gordon, "Evidence for Klein tunneling in graphene p-n junctions," Phys. Rev. Lett. **102**, 026807 (2009).
36. G. A. Steele, G. Gotz, and L. P. Kouwenhoven, "Tunable few-electron double quantum dots and Klein tunnelling in ultraclean carbon nanotubes," Nat. Nanotechnol. **4**, 363–367 (2009).
37. R. Gerritsma, B. P. Lanyon, G. Kirchmair, F. Zähringer, C. Hempel, J. Casanova, J. J. Garcya-Ripoll, E. Solano, R. Blatt, and C. F. Roos, "Quantum simulation of the Klein paradox with trapped ions," Phys. Rev. Lett. **106**, 060503 (2011).
38. O. Bahat-Treidel, O. Peleg, M. Grobman, N. Shapira, M. Segev, and T. Pereg-Barnea, "Klein tunneling in deformed honeycomb lattices," Phys. Rev. Lett. **104**, 063901 (2010).
39. D. Ö. Güney and D. A. Meyer, "Negative refraction gives rise to the Klein paradox," Phys. Rev. B **79**, 063834 (2009).
40. J. Otterbach, R. G. Unanyan, and M. Fleischhauer, "Confining stationary light: Dirac dynamics and Klein tunneling," Phys. Rev. Lett. **102**, 063602 (2009).
41. C. Bai, Y. Yang, and X. Zhang, "Effect of electron-electron interactions on the Klein paradox in graphene-based double-barrier structures," Phys. Rev. B **80**, 235423 (2009).
42. O. Bahat-Treidel and M. Segev, "Nonlinear wave dynamics in honeycomb lattices," Phys. Rev. A **84**, 021802 (2011).

43. T. Pertsch, T. Zentgraf, U. Peschel, A. Bräuer, and F. Lederer, "Anomalous refraction and diffraction in discrete optical systems," Phys. Rev. Lett. **88**, 093901 (2002).
44. A. A. Sukhorukov and Y. S. Kivshar, "Discrete gap solitons in modulated waveguide arrays," Opt. Lett. **27**, 2112–2114 (2002).
45. S. Longhi, "Photonic analog of Zitterbewegung in binary waveguide arrays," Opt. Lett. **35**, 235–237 (2010).
46. W. Greiner, *Relativistic Quantum Mechanics* (Springer-Verlag, 1990), Chap. 13.
47. A. A. Sukhorukov and Y. S. Kivshar, "Discrete gap solitons in modulated waveguide arrays," Opt. Lett. **28**, 2345–2347 (2003).